INSTITUTE OF PHYSICS PUBLISHING JOURNAL OF PHYSICS D: APPLIED PHYSICS

J. Phys. D: Appl. Phys. **39** (2006) 2775–2784 doi:10.1088/0022-3727/39/13/021

Secondary electron emission coefficients in plasma display panels as determined by particle and fluid simulations

S S Yang[1,3], S M Lee[1], F Iza[1] and J K Lee[1,2]

[1] Electronics and Electrical Engineering Department, Pohang University of Science and Technology, Pohang, Gyungbuk, 790-784, Korea

E-mail: jkl@postech.ac.kr

Received 2 March 2006
Published 16 June 2006
Online at stacks.iop.org/JPhysD/39/2775

Abstract

The secondary electron emission coefficient (γ_{se}) of ions and excited species in a plasma display panel (PDP) was studied by means of 2-dimensional fluid and 1-dimensional particle-in-cell Monte Carlo collision simulations. Relations between the driving voltage and the luminous efficiency observed in experiments are reproduced at low and high Xe concentrations. Agreement between experiments and simulations, however, requires careful selection of the γ_{se} of ions and excited species. The trend of the efficiency as a function of the driving voltage is particularly sensitive to the γ_{se} of Xe excited species. For the conditions typically encountered in PDP cells (pd= 1–10 Torr cm), the dependence of the γ_{se} on the energy of impinging ions can be neglected in discharges of pure gases. This is a consequence of multiple charge exchange collisions in the cathode region. In Xe–Ne mixtures, however, the ion energy distribution function on the cathode depends on the mixture ratio. Typically more energetic ions can reach the cathode in gas mixtures and the γ_{se} is enhanced.

(Some figures in this article are in colour only in the electronic version)

1. Introduction

The plasma display panel (PDP) is one of the leading devices for high-definition (HD) flat panel displays with diagonals over 40 inches [1]. New cell structures, manifold driving schemes and the use of high Xe concentration have solved to some degree the low luminous efficiency and high power consumption problems of older PDPs. The current performance of PDPs, however, does not guarantee supremacy over other promising display technologies such as liquid crystal display (LCD), projection and organic light emitting diode (OLED) [2]. A PDP consists of a few million cells, each representing a sub-pixel. Each cell is a micro-size dielectric barrier discharge with a small discharge volume. Its principle of light emission is analogous to that of a fluorescent lamp, i.e. ultra-violet (UV) radiation emitted by excited species in the plasma is converted to visible light by a phosphor. Some experiments have presented valuable information on the discharge behaviour by analysing the emitted UV or infrared (IR) light. Direct experimental access to plasma discharge, however, has many limitations. Typically, the length of a PDP cell is on the order of 1 mm and the discharge lasts only for 1–2 μs. In high resolution PDPs the length is reduced to just a few hundred micrometres. Overcoming the spatial and temporal experimental challenges, numerical simulation has facilitated PDP research [3–9]. Despite the difficulty and limitations of modelling, numerical simulations can provide valuable physical information that cannot be obtained experimentally. In addition, simulations can predict experimental results and guide the design of improved performance devices.

The secondary electron emission coefficient γ_{se} is a parameter that plays an important role in determining the gas breakdown voltage as well as overall characteristics of the discharge. The exact value of the γ_{se} in a real device, however, is unknown, so its value must be estimated in

[2] Author to whom any correspondence should be addressed.
[3] Present address: PDP Research Lab., PDP Division, 184 Gongdan-dong, Gumi, GyoungBuk, 730–030, Korea.

numerical simulations. There have been many experiments and theoretical approaches to find the values of γ_{se} for MgO and other protective materials in PDPs [10–13]. Different γ_{se} values have been obtained in these experimental and theoretical works, and the studies are inconclusive. In a real PDP cell, the effective secondary electron emission coefficient is a combination of the γ_{se} induced by ions, excited species and visible photons [12]. Typically, the γ_{se} of Ne ions is set to 0.3–0.5, and the γ_{se} value of Xe ion is assumed to be a tenth of that of Ne ions. For molecular ions, it is assumed to be 0.5–1 times that of the atomic ions. The values for excited species and photons are even less well known. These uncertainties influence the simulation results. In this case, quantitative and qualitative comparison of simulation results with different values of γ_{se} and experimental data can provide a means to determine the γ_{se} in a real device. Hur *et al* [14] have estimated the effective γ_{se} of the MgO layer by comparing simulated Paschen breakdown curves obtained using a 2-dimensional fluid model with experimental data from a PDP cell and presented it as a function of reduced electric field strength (E/p). The γ_{se} depends on the energy and angle of particles impinging on the surface. Since velocity information for each impinging particle is not available in fluid models, fluid simulations typically use a constant γ_{se}. It is possible, however, to consider an angle- and energy-dependent γ_{se} for impinging ions by combining the fluid simulation with data obtained in particle-in-cell (PIC) Monte-Carlo collision (MCC) simulations.

In this paper, the γ_{se} of ions and excited species in a PDP cell are estimated by comparing simulation results obtained with a 2-dimensional fluid code with experimentally measured data. Particular attention is paid to the contribution of Xe excited species. Paschen breakdown curves obtained using PIC–MCC simulations that account for the angle and energy dependence of the γ_{se} are also presented. The effect of angle and energy dependent γ_{se} in Ne–Xe mixtures is also discussed.

2. Two-dimensional fluid simulations

2.1. Reproduction of voltage versus efficiency trends

To maintain a stable sustained discharge with a low driving voltage and a large UV emission, early PDP cells used Xe–Ne mixtures with a Xe concentration of 4–5%. The Xe concentration has been increased in recent designs to levels around 10% as a way of improving efficiency and brightness. Chung *et al* [15] and Oversluizen *et al* [16] have experimentally measured the relation between the driving voltage and the luminous efficiency in PDP cells. Although similar coplanar-type PDP cells were used in the experiments, some discrepancies were observed between the two studies. At low Xe concentrations, the luminous efficiency decreases or levels off as the driving voltage is increased. On the other hand, at high Xe concentrations, U-shaped [15] or linearly increasing [16] trends are observed. Our 2-dimensional fluid simulations can reproduce both experimental observations and suggest that this behaviour is due to different values of the secondary electron emission coefficient γ_{se}.

Figures 1(*a*) and (*b*) show the simulation domain and the driving pulse shapes, respectively, for a 2-dimensional fluid simulation. The cell width in the x direction and height

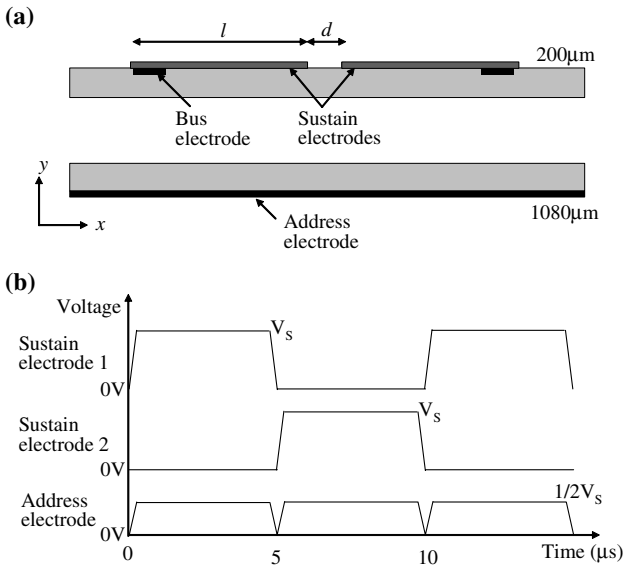

Figure 1. (*a*) Simulation domain and (*b*) driving pulse shapes applied to three electrodes for 2-dimensional fluid simulation of PDP.

in the y direction are 1080 μm and 200 μm, respectively. The thickness of the upper and lower dielectric layers is 30 μm and their relative dielectric constant ($\varepsilon/\varepsilon_0$) is 10. The thickness of the MgO and phosphor layers is ignored and their characteristics (e.g. secondary electron emission coefficient γ_{se} and the conversion rate of UV to visible photons) are included in the upper and lower dielectrics, respectively. The gap distance d between the two sustain electrodes is 80 μm and the length l of one sustain electrode is 320 μm [15]. The sustain electrodes are made of transparent materials with low electrical conductivity and bus electrodes are used to provide a low resistance path for driving the sustain electrodes (figure 1(*a*)). The frequency of the driving pulse is 100 kHz with a 50% duty ratio on each sustain electrode. The rising and falling times of all pulses are 200 ns. For the static behaviour analysis of a PDP cell, the address electrode is biased to half the applied voltage on the powered sustain electrode. Although a floating electrode can be simulated in our 2-dimensional code, the simulation time of the Poisson solver increases but no significant differences are observed with respect to the biased case. The secondary electron emission of the phosphor layer is ignored in the simulations.

First, we varied the γ_{se} of excited Xe and Ne atoms to observe the changes in plasma characteristics for a Xe 10%–Ne mixture at a gas pressure of 400 Torr. The γ_{se} values of Ne and Xe ions were set to 0.5 and 0.05, respectively. The γ_{se} values of molecular ions (Xe_2^+, Ne_2^+ and $NeXe^+$) were fixed to one fourth of those of the atomic ions. Figure 2 shows the luminous efficiency as a function of driving voltage (V_S in figure 1(*b*)) for different γ_{se} of excited species. Curve A is obtained when Xe and Ne excited species have the same γ_{se} as the atomic ions. In curves B, C and D, the γ_{se} of Xe and Ne excited species are 1/4, 1/8 and 1/12 of those of the atomic ions, respectively. Curve E is obtained when the γ_{se} of the excited species is zero. When the γ_{se} of excited species is the same as those of atomic ions, the luminous efficiency increases gradually with the driving voltage (curve A). On

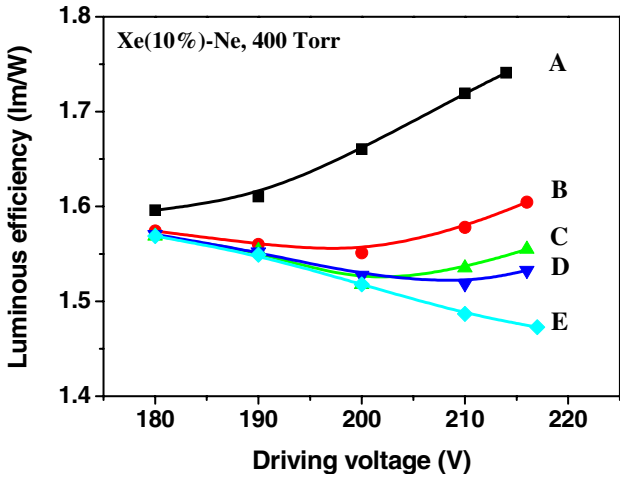

Figure 2. Transition of luminous efficiency as a function of driving voltage with five different γ_{se} values of excited species.

the other hand, when the γ_{se} of excited species is zero, the luminous efficiency decreases with increasing driving voltage (curve E). For intermediate cases (curves B to D), the luminous efficiency first decreases with increasing driving voltage, then reaches a minimum and finally increases slightly. Since Xe excited atoms outnumber the Ne excited atoms, the different trends can be attributed to the γ_{se} of Xe excited species. No significant changes are observed if only the Ne excited species γ_{se} is changed while a similar trend is obtained when only the Xe excited species γ_{se} is changed. It should be mentioned that when the γ_{se} of molecular ions is increased to one half of those of atomic ions the luminous efficiency improves. The trend of the efficiency versus voltage curve, however, does not change.

Based on this preliminary study, we were able to reproduce the voltage versus efficiency trends obtained experimentally. Figures 3 and 4 present the simulation results for Xe–Ne mixtures with Xe concentration of 5% and 10%, respectively, and a total pressure of 400, 500 and 600 Torr. In these simulations, the γ_{se} of atomic Ne and Xe ions were 0.5 and 0.05, respectively, and the γ_{se} of molecular ions was fixed to one fourth of that of atomic ions. For the Xe and Ne excited species, 1/12 of the γ_{se} of the atomic ions was used as presented in the preliminary study. Figures 3(*a*) and 4(*a*) show the transition of luminous efficiency as a function of driving voltage, while figures 3(*b*) and 4(*b*) are the change of luminance. In agreement with the experimental measurements, luminance increases linearly as the driving voltage increases both at low (5%) and high (10%) Xe concentrations. Luminous efficiencies, however, show different trends at low and high Xe partial pressures, and the trends depend on the total pressure. At low Xe concentration and low gas pressure (e.g. Xe 5% and 400 Torr in figure 3(*a*)), the luminous efficiency decreases linearly in spite of the increase in driving voltage. When the gas pressure is increased from 400 to 600 Torr, the efficiency reduction at high driving voltages becomes smaller. At high Xe concentration and low gas pressure (e.g. Xe 10% and 400 Torr in figure 4(*a*)), the luminous efficiency reduces as the driving voltage is increased in the low driving voltage region. At higher driving voltages, however, the luminous efficiency increases with the driving voltage. As the gas pressure increases, U-shaped luminous efficiency curves can be clearly identified.

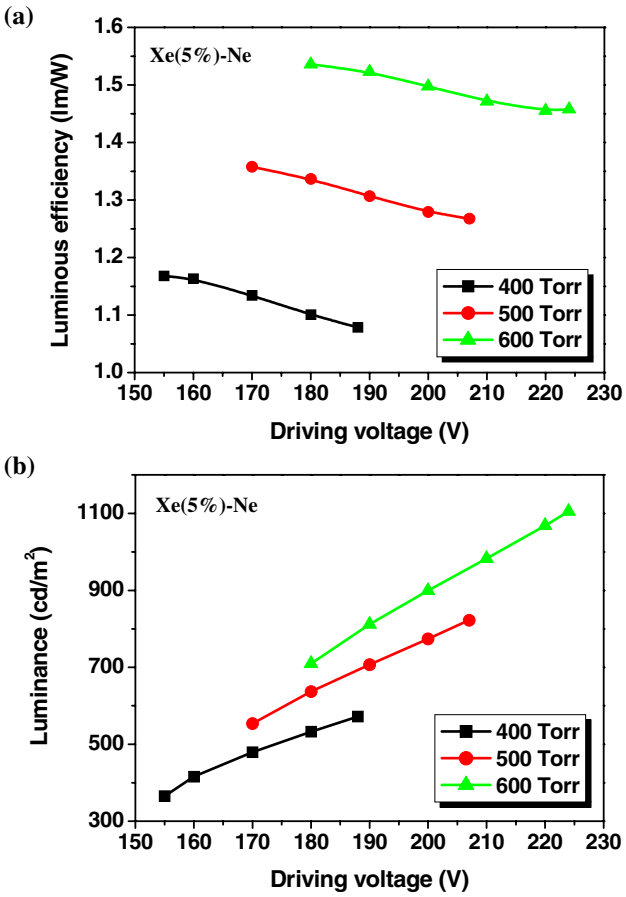

Figure 3. (*a*) Luminous efficiency and (*b*) luminance as a function of driving voltage at low Xe concentration (Xe 5%–Ne) with varying gas pressures. The γ_{se} values of Ne and Xe ions are 0.5 and 0.05, respectively. The γ_{se} value of excited species is 1/12 of the γ_{se} value for atomic ions.

These simulation results (figures 3 and 4) agree well with the experimental measurements reported in [15].

This voltage versus efficiency trend depends on the γ_{se} values of atomic ions and excited species. Figures 5(*a*) and (*b*) show the luminous efficiency as a function of driving voltages at low and high Xe concentrations obtained in another simulation with different secondary electron emission coefficients. In this simulation, the γ_{se} of Ne and Xe atomic ions were reduced to 0.3 and 0.02, respectively, while other γ_{se} values were the same as those in the previous simulation (figures 3 and 4). Although the reduction of γ_{se} caused a reduction in luminous efficiency, a similar trend with driving voltage is observed at low Xe concentration. (Compare figure 3(*a*) and figure 5(*a*).) At high Xe concentration, however, the reduction in luminous efficiency is accompanied by a change in trend. (Compare figure 4(*a*) and figure 5(*b*).) Instead of U-shaped curves, the luminous efficiency increases monotonically with increasing pressure.

Figure 6 shows a comparison of the efficiency versus voltage trends obtained with different γ_{se} of excited species. The γ_{se} values of Ne and Xe atomic ions were kept to 0.3 and 0.02, respectively. Xe–Ne mixtures with 5% and 10% Xe at a gas pressure of 500 Torr were used in these simulations. When the γ_{se} value of excited species was increased from 1/12

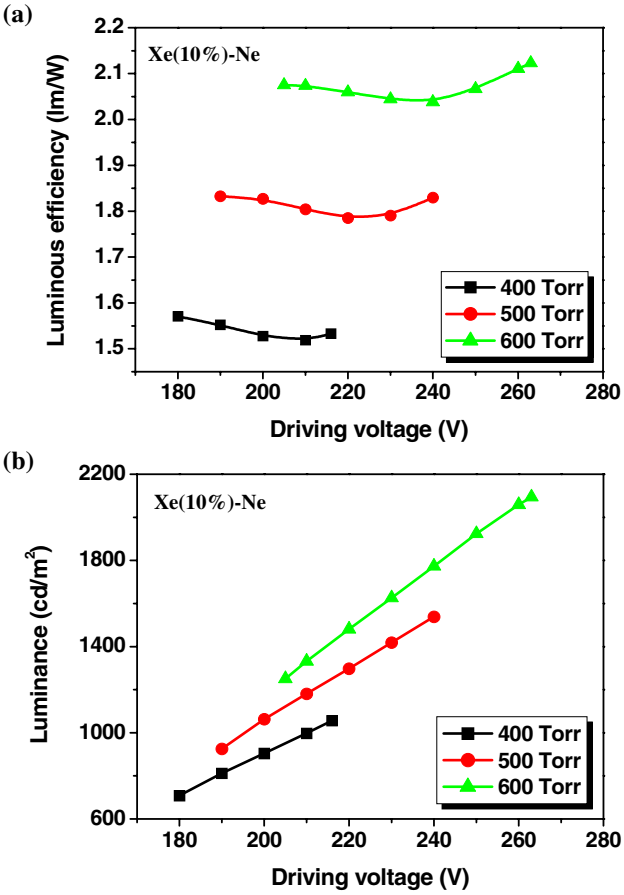

Figure 4. (*a*) Luminous efficiency and (*b*) luminance as a function of driving voltage at high Xe concentration (Xe 10%–Ne) with the variation of gas pressure. The same γ_{se} values for ions and excited species as the low Xe concentration case are used.

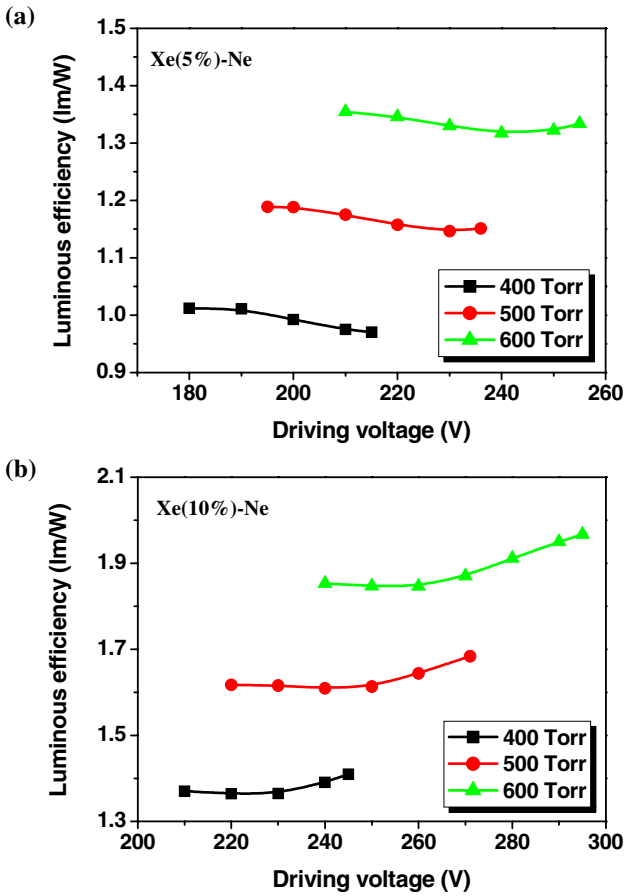

Figure 5. Luminous efficiency as a function of driving voltage at (*a*) low and (*b*) high Xe concentrations with varying gas pressures. The γ_{se} values of Ne and Xe atomic ions are changed to 0.3 and 0.02, respectively.

(squares) to 1/4 (circles) of that of the atomic ions, the luminous efficiency increased. More significant is the drastic change in the overall trend, especially in the high driving voltage region. A U-shaped curve previously only observed in the high Xe case is now also observable in the low Xe concentration case. This trend is similar to the experimental data reported in [16]. In addition, our fluid simulations show that $Xe^*(^3P_2)$ is the excited species with the most influence on the efficiency versus voltage curve.

The simulation results are in good qualitative agreement with the different trends of the luminous efficiency versus driving voltage observed in experiments [15, 16]. Although a good quantitative agreement is also found with experimental data reported in [15], the variation of the luminous efficiency observed in experiments [16] is larger than that obtained in our simulations. The quantitative disagreement is attributed to differences in the PDP cell specification, the simulation dimensions and uncertainties of plasma parameters in the fluid simulation. Previous works have suggested that the discharge characteristics depend weakly on the γ_{se} [16–18] and therefore further research is needed to fully understand the voltage dependence of the efficiency.

Based on our fluid simulations, we can conclude that the trend of the efficiency versus driving voltage is influenced by the secondary electron emission coefficients of ions and excited species impinging on the MgO layer. Depending on the manufacturing and ageing processes of the PDP cell, the surface conditions of the MgO layer and its characteristics can vary significantly. These variations can produce different trends in the efficiency versus driving voltage in different test panels and even among different cells within one panel. By comparing experimental data with these fluid simulation results, we can investigate the change of the γ_{se} values of the MgO layer by ions and excited species as a function of time.

2.2. *Analysis of efficiency transition*

The transition from a negative slope to a positive slope in the efficiency versus voltage curves can be analysed in terms of the electron heating efficiency (η_e) and the Xe excitation efficiency (η_{exc}). The discharge efficiency (η_{dis}) can be calculated approximately as the product of η_e and η_{exc} as follows [15, 17, 18]:

$$\eta_{dis} = \frac{W_{UV}}{W_{in}} \sim \frac{W_{exc}}{W_e} \times \frac{W_e}{W_{in}} = \eta_{exc} \times \eta_e, \qquad (1)$$

where W_{UV} and W_{in} are the total energy of UV photons and the total energy dissipated in the discharge, respectively. W_e is the energy delivered to the electrons and W_{exc} the energy spent by the electrons in exciting Xe species. Figure 7 shows the

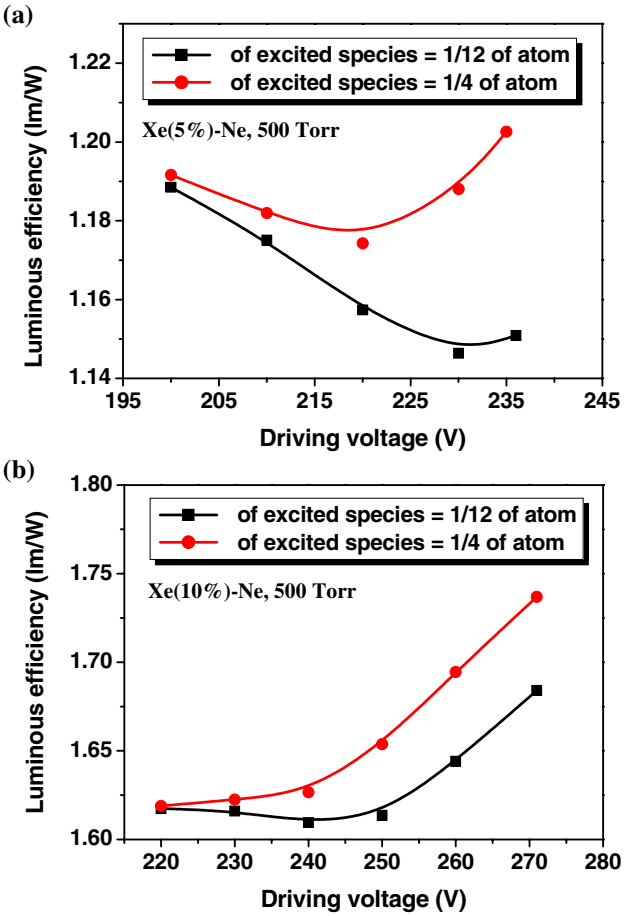

Figure 6. Comparison of voltage versus efficiency trends of low and high γ_{se} values of excited species at (*a*) low and (*b*) high Xe concentrations.

diagrams of the total input energy flow and the electron energy flow in inelastic processes for two gas conditions. Here Xe**, which represents the sum of several high energy level states [19], generates other lower energy level excited species upon collision with other species. Figures 7(*a*) and (*c*) correspond to a low Xe concentration (5%) discharge at low pressure (400 Torr) and figures 7(*b*) and (*d*) to a high Xe concentration (10%) discharge at high pressure (600 Torr). Approximately half the input energy is delivered to the electrons, and η_e shows a slight increase with the driving voltage in both cases (figures 7 and 8). As the driving voltage is increased, the electric field in the discharge region increases, leading to an increase in the fractional energy spent in ionizing Ne. The increase in the relative number of Ne ions, which have a higher γ_{se} than Xe ions, increases the emission of secondary electrons on the cathode surface and improves the electron efficiency (η_e).

With regarding to the Xe excitation efficiency (η_{exc}), however, two different trends are observed for the two gas conditions presented in figures 7 and 8. For both gas conditions, as the driving voltage is increased, the relative electron energy spent in ionization processes increases and that in the excitation processes reduces. At low Xe concentration and low pressure, the reduction of η_{exc} is larger than the increase in η_e, and consequently the discharge efficiency ($\eta_e\eta_{exc}$) decreases as the driving voltage increases (figure 8(*a*)). At high Xe concentration and high pressure, however, the relative electron energy spent in ionization initially increases but then levels off (figures 7(*d*) and 8(*b*)). As a result, the discharge efficiency as a function of the driving voltage shows a U-shaped trend (figure 8(*b*)) similarly to the luminous efficiency in figure 4(*a*).

3. One-dimensional PIC–MCC simulations

3.1. Angle and energy dependence of γ_{se}

The secondary electron emission coefficient (γ_{se}) depends in general on the energy and angle of the impinging particle. In the previous fluid simulations, we investigated the effective secondary electron emission coefficient of various species impinging on the MgO layer. This value represents an average (over the particle distribution function) value. To investigate the influence of the energy and angle of the incident ions, we have compared theoretical Paschen breakdown curves with those obtained with a 1-dimensional PIC–MCC simulation code (XPDP1 [20]) and our fluid code. The original XPDP1 code uses a constant γ_{se}. In order to model the angle and energy dependence of the γ_{se}, a suitable model for gases typically used in PDP cells impinging on MgO is needed. Phelps and Petrovic [21] developed a model for the secondary electron production yields by Ar ions impinging on targets with several surface conditions. 1-dimensional PIC simulation results done by Radmilović-Radjenović and co-workers [9, 22] using this model showed an improved agreement with experimental measurements in capacitively coupled plasma and micro-gap systems. However, it is not easy to obtain reliable energy dependent secondary electron yields by He, Ne and Xe ions (species widely used in PDPs) on the metallic cathode and the MgO layer.

Lee *et al* [13] have measured the secondary electron emission yield from the MgO thin layer as a function of the ion kinetic energy for five noble gas ions (He, Ne, Ar, Kr and Xe) using a pulsed ion beam technique. Unfortunately, due to the limitation of the experiment, the secondary electron emission yields in the energy range below 50 eV could not be measured. In our simulations we use their experimental data and extrapolate it as needed. The secondary electron emission coefficient is assumed to be of the form [23]

$$\gamma_{se}(\varepsilon_i) = a + 0.000\,03 \times \varepsilon_i^b \qquad (2)$$

where a and b are constants and ε_i is the energy of the incident ion. Figure 9 shows the experimental data [13] (symbols) and the numerical fit (solid line) obtained using equation (2). The squares, circles and triangles are the experimentally measured secondary electron yields for He, Ne and Xe ions, respectively. The set of constants (a, b) used in equation (2) are (0.274, 1.754) for He, (0.2, 1.65) for Ne and (0.01, 1.455) for Xe. For Xe, the fit to experimental data requires (a, b) equal to $(-0.0365, 1.455)$. A negative value of a means that there is a threshold below which the secondary electron emission coefficient is zero. For numerical reasons, instead of using the direct fit, we have modified it by increasing a to 0.01 as shown in figure 9. For the constant γ_{se} simulations, the γ_{se} for He, Ne and Xe ions are set to 0.273, 0.2 and 0.01, respectively. These are the γ_{se} values for ions incident with zero energy, i.e. $\varepsilon_i = 0$.

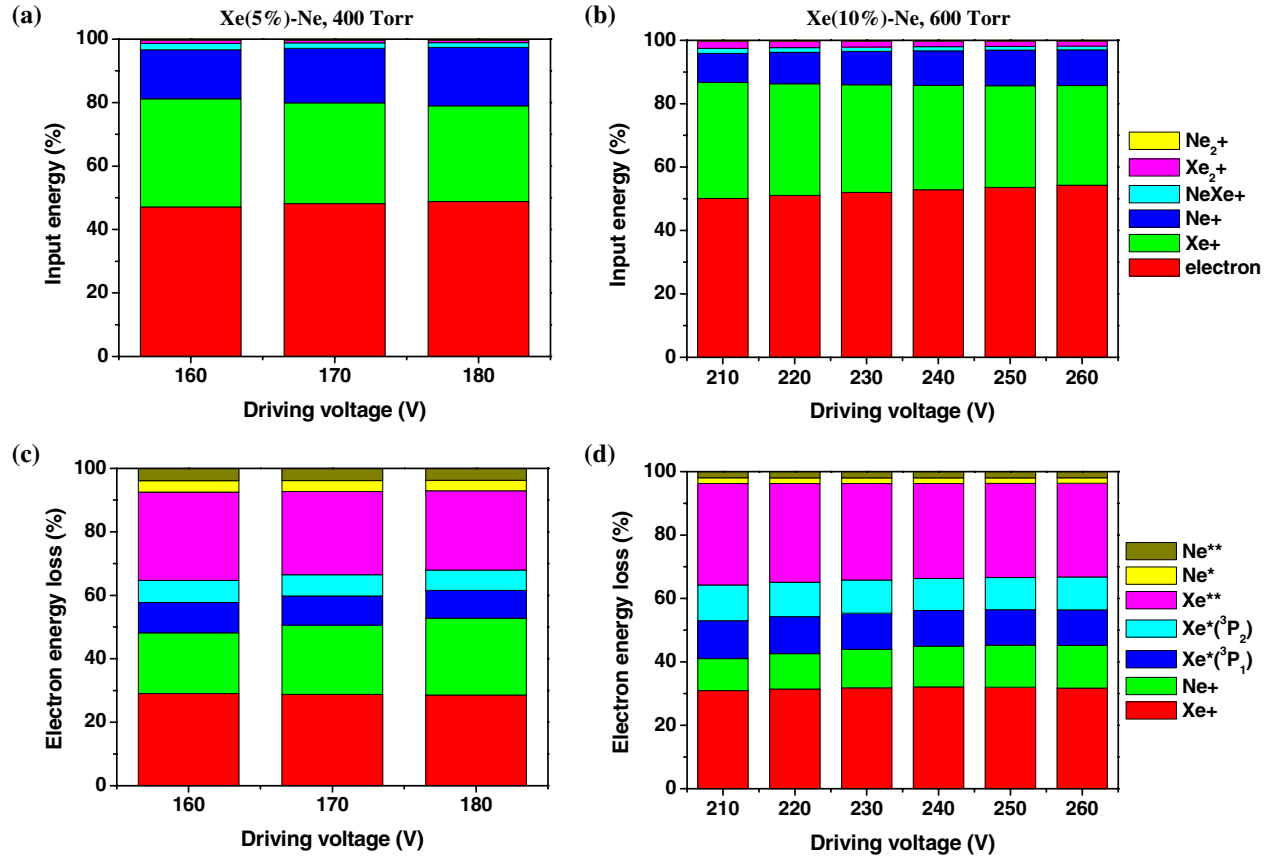

Figure 7. Diagrams of input energy and inelastic electron energy loss for (*a* and *c*) Xe 5%–Ne at 400 Torr and (*b* and *d*) Xe 10%–Ne at 600 Torr.

The dependence of the γ_{se} on the angle of the incident ions is combined with the energy dependence as [9, 24, 25]

$$\begin{aligned} \gamma_{se}(\varepsilon_i, \theta) &= \gamma_{se}(\varepsilon_i)\cos^{-1}\theta \qquad \text{for } \theta < 60^\circ, \\ \gamma_{se}(\varepsilon_i, \theta) &= \gamma_{se}(\varepsilon_i)\cos^{-1}(60^\circ) \qquad \text{for } \theta \geqslant 60^\circ, \end{aligned} \tag{3}$$

where θ is the incident angle of impinging ions and $\theta = 0^\circ$ means that a particle impinges on the surface perpendicularly.

3.2. Paschen breakdown curve

The voltage at which a gas confined in a gap between two plane–parallel metallic electrodes ignites is a function of the total gas pressure (p) and the gap size (d). This voltage is called the breakdown voltage, a given γ_{se} (gas and electrode material) and first Townsend coefficient α(gas) and the breakdown voltage is a function of the pd value. Generally it is assumed that the first Townsend coefficient can be expressed as [26]

$$\alpha = Ap\exp(-Bp/E), \tag{4}$$

where E and p are the magnitude of the electric field and gas pressure, respectively. A and B are constants determined by experimental approximation which are roughly constants over a range of electric field for any given gas [26]. This assumption has been widely used in the theoretical analysis of the breakdown voltage. By using this first Townsend coefficient and the self-sustaining condition, the Paschen breakdown voltage is given by

$$V_f = \frac{Bpd}{\left(\ln\dfrac{Apd}{\ln(1+(1/\gamma_{se}))}\right)}. \tag{5}$$

For inert gases such as He, Ne, Ar, Kr and Xe, however, equation (4) is not the best approximation. Instead the first Townsend coefficient is better approximated by [26]

$$\alpha = Cp\exp(-D(p/E)^{1/2}), \tag{6}$$

where the constants C and D are different from the constants A and B used in equation (4). Using this formula for the first Townsend coefficient, the breakdown voltage is given by

$$V_f = \frac{D^2pd}{\left(\ln\dfrac{Cpd}{\ln(1+(1/\gamma))}\right)^2}. \tag{7}$$

We shall refer to equations (5) and (7) as the 1st and 2nd theoretical Paschen breakdown curves, respectively.

These theoretical Paschen breakdown curves have been compared with 1-dimensional PIC–MCC simulation results considering the angle and energy dependent γ_{se} values of incident ions. For the dc breakdown, a simple parallel electrode configuration was considered. The gap distance between the two parallel electrodes was fixed at 100 μm and the gas pressure varied between 100 to 1000 Torr. The time step

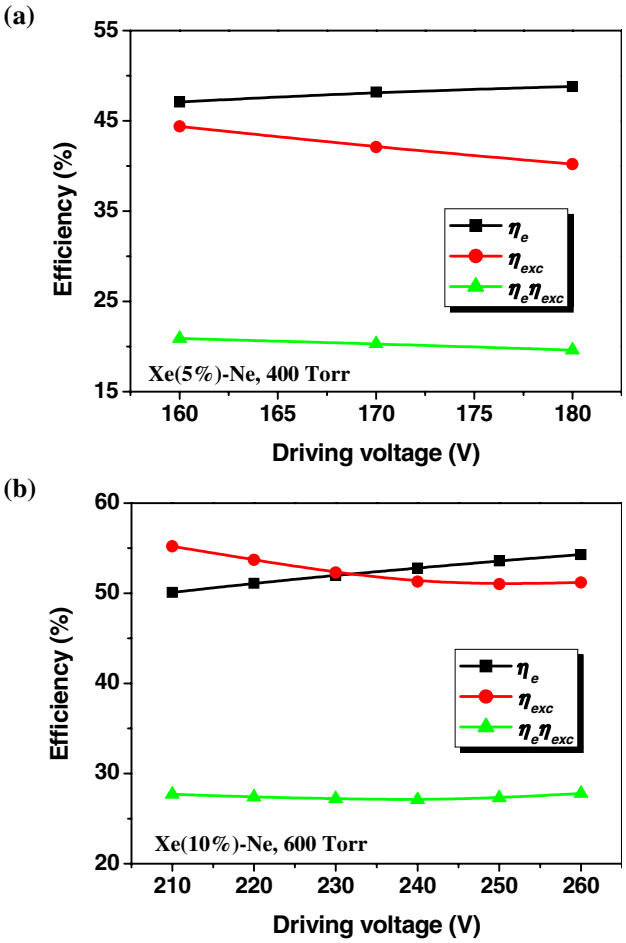

Figure 8. Electron heating (η_e) and Xe excitation efficiency (η_{exc}) at (*a*) Xe 5%–Ne at 400 Torr and (*b*) Xe 10%–Ne at 600 Torr.

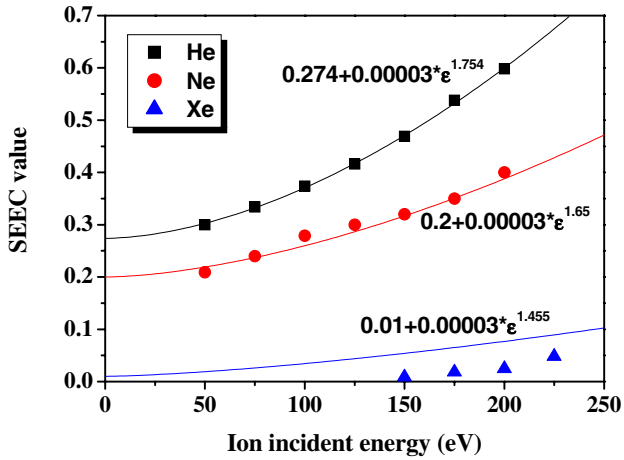

Figure 9. Experimentally measured γ_{se} values (symbols) in [13] and fitted data (solid lines) for simulations as a function of ion incident energy for pure He, Ne and Xe gases.

Δt and the number of spatial cells were 10^{-14} s and 500, respectively. The density at the beginning of the simulation is 10^{18} m^{-3} and the number of physical particles per computer particle 10^4. The electrodes are assumed to be coated with MgO and therefore to have the ion energy dependent γ_{se} shown in figure 9.

For these simulations, the collision cross-sections of He, Ne and Xe gases were added to the original XPDP1 code. Figures 10(*a*)–(*c*) show the electron collision cross-section as a function of the electron energy for elastic scattering (ES), excitation (EX), and ionization (IZ) with He, Ne and Xe neutrals, respectively [27]. The excitation cross-section is the sum of several dominant excited states. Figure 10(*d*) shows the collision cross-sections as a function of ion energy for ion ES and resonant (or symmetric) charge exchange (CX) for He, Ne and Xe ions in their parent gases [26, 28]. Non-resonant CX collisions between different species were not taken into account in these PIC simulations. CX collisions in the cathode sheath are important in determining the mobility and energy of the ions. In a pure gas discharge, the CX collisions dominate elastic collisions. In gas mixtures such as Xe–Ne, however, the dominant collision is determined by the ratio of gases.

Figure 11 compares the theoretical Paschen breakdown curves for Ne (equations (5) and (7)) with 1-dimensional PIC and 2-dimensional fluid simulations at typical *pd* values encountered in PDPs (1–10 Torr cm). The solid lines representing the 1st and 2nd theoretical Paschen breakdown curves show some differences. The square symbols correspond to the data obtained from our 2-dimensional fluid simulation. A constant γ_{se} of 0.2 was used in the fluid simulation, and three cases were investigated using the 1-dimensional PIC–MCC code.The diamonds correspond to PIC simulation results with a constant $\gamma_{se}(= 0.2)$, circles to simulation results with an energy dependent γ_{se} and triangles to those with an angle and energy dependent γ_{se}. While the fluid simulation agrees well with the theoretical Paschen curves, the PIC–MCC simulations have some discrepancies. The trend of the Paschen curve, however, is obtained in both cases. The theoretical curves predict a minimum breakdown voltage V_{min} at *pd* values of 1–2 Torr cm. In PIC simulations, the V_{min} is shifted to higher *pd* values ($\sim$ 3 Torr cm). The PIC–MCC simulations show that for a pure Ne discharge, the ion incident energy does not affect the γ_{se} value. In figure 11, the simulation results obtained with a constant γ_{se} overlap those obtained with an energy dependent γ_{se}. This indicates that Ne ions impinging on the cathode surface have very low energies as a result of frequent CX collision between Ne ions and Ne neutrals in the cathode sheath. Since the total gas pressure in a PDP cell is around a few hundred Torr, the mean free path of the ion is about 1 μm, and resonant CX collisions between ions and neutrals occur frequently in the cathode sheath. New ions generated by CX collision can be accelerated only through the remainder of the sheath potential. Therefore the energy of the ions impinging on the cathode decreases as the number of CX collisions increases. The analysis of the energy distributions of impinging ions obtained by 1-dimensional PIC–MCC simulations show that the probability of ions hitting the cathode with energies larger than 30 eV is negligible. As shown in figure 9, there is no significant difference in the γ_{se} value for Ne ions in the energy range 0–25 eV. On the other hand, when the angle dependent γ_{se} value is applied, the breakdown voltage reduces by 3–7 V. The angle distribution function of ions striking the cathode has a peak at 3°–4° and 90% of the ions impinge on the surface with an incident angle below 30°. In 1-dimensional simulations, because the cathode is opposite to the anode, the direction of the electric field at the cathode sheath region is normal to

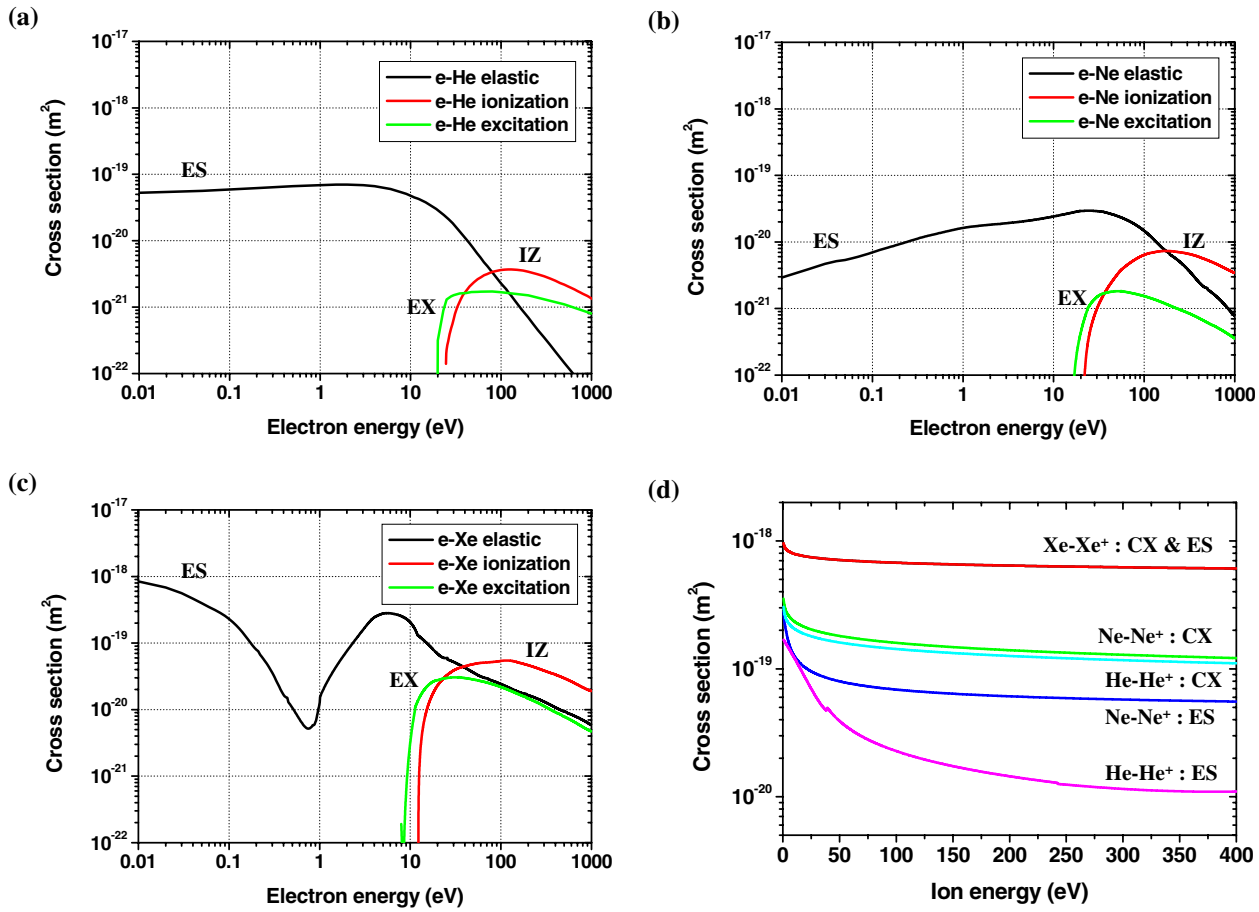

Figure 10. Collision cross-section of (*a*) ES, (*b*) excitation (EX) and (*c*) ionization (IZ) between electron-neutral and of (*d*) resonant CX and ES by ion-neutral for He, Ne and Xe gases.

the dielectric surface. As shown by Yang *et al* [29] using 2-dimensional PIC code, however, this angle distribution is not representative of a coplanar-type PDP cell.

Figure 12 shows breakdown voltage curves for He. In this case, 1-dimensional PIC–MCC simulation results agree better with the 2nd theoretical Paschen breakdown curve. The breakdown voltage data of pure He from experimental measurement done by Postel and Capelli [30] (square symbols in figure 12) are also consistent with those of our 1-dimensional PIC simulations. Although He ions have a higher γ_{se} than Ne ions, our simulations show that the breakdown voltage of He is higher than that of Ne. For a *pd* value of 5 Torr cm and a driving voltage of 153 V, the time averaged γ_{se} values for constant, energy dependent, and angle and energy dependent secondary emission coefficients are 0.27475, 0.27609 and 0.29627, respectively. Like the pure Ne case, ions striking the cathode in a pure He discharge have little energy and no significant increase in the γ_{se} is observed when the energy dependent γ_{se} only is considered.

3.3. Ion energy dependent γ_{se} value in gas mixture

Unlike pure gases, in Ne–Xe mixtures, high energetic ions can reach the cathode and affect the γ_{se} value. Figure 13 shows the energy distributions of ions impinging on the cathode surface in two Xe–Ne mixtures at 300 Torr. Figure 13(*a*) corresponds

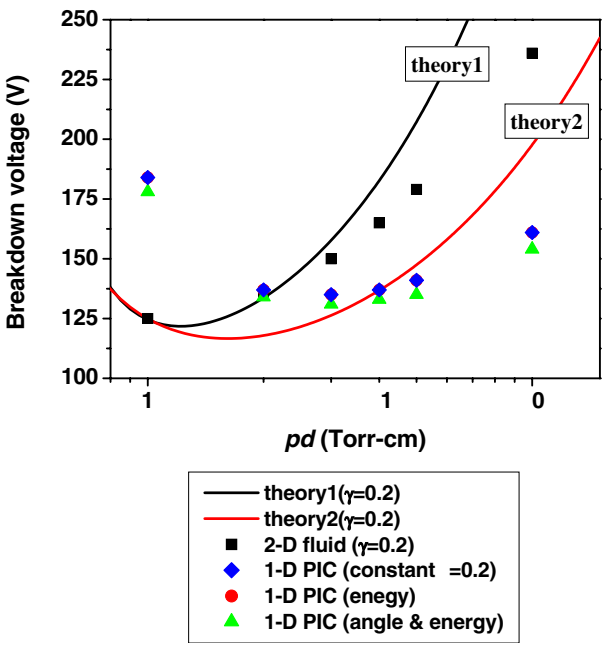

Figure 11. Paschen breakdown curves of Ne gas obtained from theories and fluid and 1-dimensional PIC simulations.

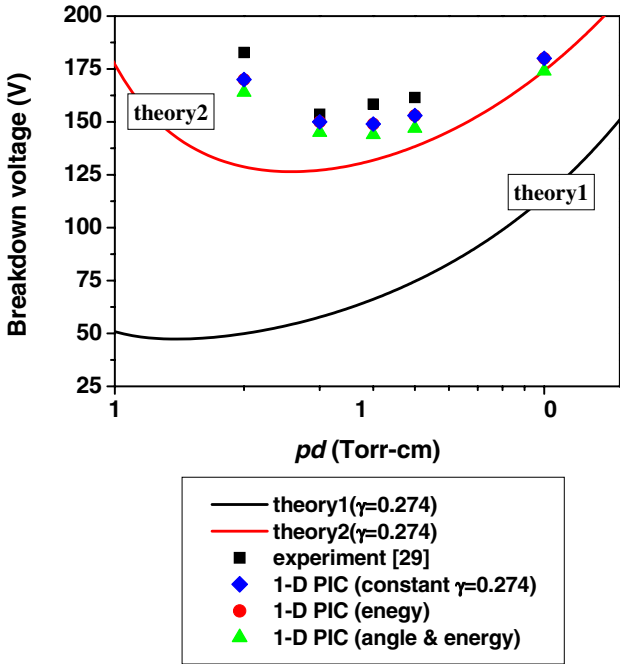

Figure 12. Paschen breakdown curves of He gas obtained from theories, experiment [28] and 1-dimensional PIC simulations.

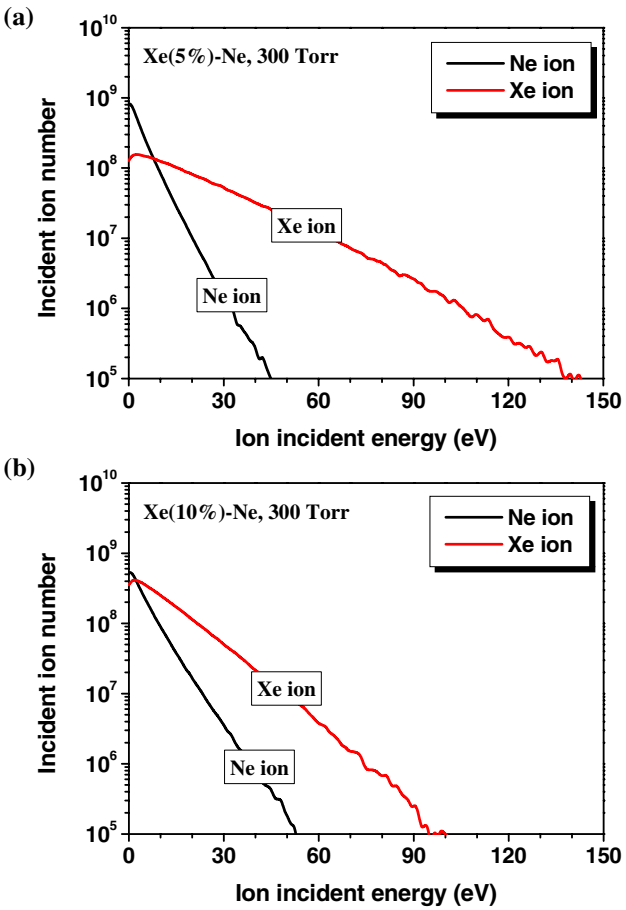

Figure 13. Incident energy distributions of Ne and Xe ions on the cathode surface at (*a*) low (Xe 5%–Ne) and high (Xe10%–Ne) Xe concentrations.

to a Xe concentration of 5% and an applied voltage of 190 V and figure 13(*b*) to a Xe concentration of 10% and an applied voltage of 200 V. Although Xe and Ne ions are accelerated by the same field in the cathode sheath, Xe ions are more energetic than Ne ions. At the low Xe concentration (5%) the partial pressure of Xe is much lower than that of Ne and the probability of resonant CX collision of Xe ions is very small (in spite of the large CX cross-section as shown in figure 10(*d*)). Therefore, many Xe ions can reach the cathode surface or MgO layer with relatively high energies. The Xe concentration determines the shape of the ion energy distributions. When the Xe concentration is increased from 5% to 10%, Xe ions experience more frequent resonant CX collisions. At the same time, the reduction to Ne partial pressure translates to a reduction in the number of CX collisions between Ne ions and Ne neutrals. As a result, when the Xe concentration is increased, the number of high energetic Xe ions reduces rapidly, while that of Ne ions increases gradually (figures 13(*a*) and (*b*)).

Therefore, due to the reduction of resonant CX collisions, the energy of the ions bombarding the cathode surface is larger in Xe–Ne mixture discharges than in a pure Xe or pure Ne discharge. The more energetic ion bombardment enhances the secondary electron emission in mixture discharges. The averaged (over the energy distribution of impinging ions) γ_{se} for Ne ions in mixture discharges with 5% and 10% Xe is 0.7% and 3%, respectively, larger than in a pure Ne discharge. On the other hand, for Xe ions the γ_{se} decreases as Xe concentration is increased. For 5% Xe and 10% Xe mixtures, the averaged energy-dependent γ_{se} is 21% and 15%, respectively, larger than that in a pure Xe discharge.

4. Conclusion

Two types of luminous efficiency versus driving voltage trends observed in experiments have been reproduced in 2-dimensional fluid simulations. The agreement requires adjusting the secondary electron emission coefficients (γ_{se}) of ions and excited species. The simulation results provide a better understanding of the mechanisms determining the luminous efficiency in a PDP cell and can be used to infer the secondary electron emission coefficient in a cell as it ages. The luminous efficiency in a cell with low Xe concentration and at low pressure decreases with increasing driving voltage. On the other hand, the luminous efficiency in a cell with high Xe concentration and at high gas pressure increases with increasing driving voltage. The trend of the efficiency as a function of the driving voltage, however, is very sensitive to the effective γ_{se} of ions and excited species. Simulation shows that Xe excited atoms, especially Xe*($^3P_2$), have the most profound effect on the shape of the efficiency versus voltage curve.

The variation of the γ_{se} as a function of the energy and angle of the impinging ions has also been studied by means of 1-dimensional PIC simulations with MCC. For typical conditions encountered in PDP cells (pd = 1–10 Torr cm) and for discharges in pure gases, the γ_{se} can be modelled as a constant. In this case, multiple CX collisions in the cathode sheath prevent ions from gaining energy. In Xe–Ne mixtures, however, the energy distributions of Xe and Ne ions impinging on the cathode surface depend on the mixture ratio, and the

presence of energetic ions enhances the secondary electron emission with respect to the pure gas case.

Acknowledgment

This work was supported by LG Electronics and LG Micron.

References

[1] Lee J K and Verboncoeur J P 2001 *Low Temperature Plasma Physics* ed R Hippler *et al* (Berlin: Wiley-VCH) pp 367–85
[2] Weber L F 2005 *Proc. 5th Int. Meeting on Information Display (Seoul, Korea)* p 3
[3] Sahni O, Lanza C and Howard W E 1978 *J. Appl. Phys.* **49** 2365–75
[4] Punset C, Cany S and Boeuf J P 1999 *J. Appl. Phys.* **86** 124–33
[5] Rauf S and Kushner M J 1999 *J. Appl. Phys.* **85** 3460–9
[6] Lee H J, Kim H C, Yang S S and Lee J K 2002 *Phys. Plasmas* **9** 2822–30
[7] Kim H C, Hur M S, Yang S S, Shin S W and Lee J K 2002 *J. Appl. Phys.* **91** 9513–20
[8] Yang S S, Kim H C, Ko S W and Lee J K 2003 *IEEE Trans. Plasma Sci.* **31** 596–605
[9] Kim H C, Iza F, Yang S S, Radmilović-Radjenović M and Lee J K 2005 *J. Phys. D: Appl. Phys.* **38** R283–301
[10] Auday G, Guillot Ph and Galy J 2000 *J. Appl. Phys.* **88** 4871–4
[11] Motoyama Y, Matsuzaki H and Murakami H 2001 *IEEE Trans. Electron Dev.* **48** 1568–74
[12] Murakami Y, Matsuzaki H, Murakami H and Ikuta N 2001 *Japan. J. Appl. Phys.* **40** 3382–8
[13] Lee S K, Kim J H, Lee J and Whang K W 2003 *Thin Solid Films* **435** 69
[14] Hur M S, Lee J K, Kim H C and Kang B K 2001 *IEEE Trans. Plasma Sci.* **29** 861–3
[15] Chung W J, Shin B J, Kim T J, Bae H S, Seo J H and Whang K W 2003 *IEEE Trans. Plasma Sci.* **31** 1038–43
[16] Oversluizen G, Zwart S, Heusden S and Dekker T 1999 *Proc. 6th Int. Display Workshop (Sendai, Japan)* p 591
Oversluizen G, Zwart S, Heusden S and Dekker T 2000 *Proc. 7th Int. Display Workshop* p 631
[17] Hayashi D, Heusler G, Hagelaar G and Kroesen G 2004 *J. Appl. Phys.* **95** 1656–61
[18] Hagelaar G, Klein M, Snijkers R and Kroesen G 2001 *J. Appl. Phys.* **89** 2033–9
[19] Meunier J, Belenguer Ph and Boeuf J P 1995 *J. Appl. Phys.* **78** 731–45
[20] Vahedi V and Surendra M 1995 *Comput. Phys. Commun.* **87** 179–98
[21] Phelps A V and Petrović Z Lj 1999 *Plasma Sources Sci. Technol.* **8** R21–44
[22] Radmilović -Radjenović M, Lee J K, Iza F and Park G Y 2005 *J. Phys. D: Appl. Phys.* **38** 950–4
[23] Lee S K, Kim J K, Ryu J H and Lee J 2003 *Proc.* 10th *Int. Display Workshop (Fukuoka, Japan)* p 981
[24] Thieberger P, Hanson A L, Steski D B, Zajic V, Zhang S Y and Ludewig H 2000 *Phys. Rev.* A **61** 042901
[25] Radmilović-Radjenović M 2004–2005 private communication
[26] Raizer Y P 1991 *Gas Discharge Physics* (Berlin: Springer)
[27] The Siglo Database *Kinema Research & Software* http://www.kinema.com/
[28] Almeida P G C, Benilov M S and Naidis G V 2002 *J. Phys. D: Appl. Phys.* **35** 1577–84
[29] Yang S S, Lee J K, Ko S W, Kim H C and Shon J W 2004 *Contrib. Plasma Phys.* **44** 536–41
[30] Postel O B and Cappelli M A 2000 *Appl. Phys. Lett.* **76** 544–6